第33卷第6期
2014年12月

红外与毫米波学报
J. Infrared Millim. Waves

Vol. 33, No. 6
December, 2014

文章编号:1001 - 9014(2014)06 - 0571 - 06

DOI:10.3724/SP. J. 1010. 2014. 00571

Design and analysis of resonant cavity-enhanced quantum ring inter-subband photodetector with resonant tunneling barriers for terahertz detection

Mahdi Zavvari[1], Mohammad Karimi[2], Kambiz Abedi[3]

(1. Department of Electrical Engineering, Urmia Branch, Islamic Azad University, Urmia, Iran;
2. Department of Electrical Engineering, Ahar Branch, Islamic Azad University, Ahar, Iran;
3. Department of Electrical Engineering, Faculty of Electrical and Computer Engineering, Shahid Beheshti University, G. C. 1983963113, Tehran, Iran)

Abstract: The effect of resonant cavity structure on the performance operation of InAs/GaAs quantum ring inter-subband photodetector is studied for detection of terahertz radiations range. In order to confinement of optical field within active region and consequently enhancement in responsivity of device, two periods of Al_2O_3/GaAs distributed bragg reflectors are used as bottom dielectric mirror and a thin layer of Au material as top mirror of device. For further improvement in detectivity, $Al_{0.3}Ga_{0.7}As$/ $In_{0.3}Ga_{0.7}As$ resonant tunneling barriers are included in absorption layers to reduce dark current of device. Proposed photodetector shows a peak responsivity of about 0.4 (A/W) and quantum efficiency of 1.2% at the wavelength of 80 μm (3.75 THz). Furthermore, specific detectivity (D^*) of device is calculated and results are compared to conventional quantum ring inter-subband photodetector. Results predict a D^* of $\sim 10^{11}$ (cm. $Hz^{1/2}$/W) for device at $T = 80$ K and $V = 0.4$ V which is two orders of magnitude higher than that of conventional QRIPs.

Key words: quantum ring photodetector, resonant cavity, detectivity, distributed bragg reflector, resonant tunneling barrier

PACS: 32.80.Gc, 73.40.Gk, 78.40.Fy, 78.40.Ha

Introduction

Terahertz (THz) detectors are in demand due to their wide applications in the fields of medical, T-Ray imaging, spectroscopy, plasma fusion diagnostic and so on [1-2]. Different structures have been proposed for detection of THz range including quantum well infrared photodetectors (QWIP)[3], hot electron bolometers (HEB)[4], graphene terahertz photodetectors[5] and quantum dot terahertz photodetectors (QDIP)[6]. Over last decade, QDIPs have attained great attention because of their capability to detect normally incident radiations originated from 3D carrier confinement and some structures have reported [7-10]. Su *et al.* have reported tunneling self-organized $In_{0.6}Al_{0.4}As$/GaAs quantum dots as inter-sublevel photodetector with peak responsivity at ~ 50 μm[6]. Lin *et al.* have used ten period InAs-GaAs quantum dot layer inside the active region of semiconductor photodetector. They observed responsivity spectrum at 10.4 μm and 8.4 μm for the device under positive and negative biases, respectively [11]. Also, Zavvari *et al.* have reported quantum dot infrared photodetector enhanced by avalanche multiplication with high responsivity of 12 (A/W) and higher specific detectivity of approximately 6×10^9 cm. $Hz^{1/2}$/W at wavelength of 11 μm[12]. Although QDIPs have potential to detect THz range, due to size limitation of QDs, the detection spectrum is limited below 60 μm. Adding Al to InAs QDs leads to forming of InAlAs QDs with low dimensions [6], but size limitation still exist. Recently, a new quantum structure named quantum ring (QR) with very low dimensions are proposed to be used in the active region of photodetector resulting in quantum ring inter-subband photodetector which is suitable to detect virus, plastic explosive and bio- images with molecular vibration frequencies at 0.1-30 THz[13-15]. Bhowmicket al. have reported high performance quantum ring detector for 1-3 terahertz range with peak responsivity of 25 A/W, specific detectivity of 1×10^{16} cm. $Hz^{1/2}$/W at the wavelength of 165 μm (1.82 THz)[16]. Although, low dimensions of QR leads to energy levels with less spacing that makes QR based photodetectors suitable to detect very long-wavelength up to 175 μm[17], but QE of device is very low which can

Received date: 2013 - 07 - 29, **revised date**: 2014 - 10 - 08 收稿日期:2013 - 07 - 29, 修回日期:2014 - 10 - 08

Biography: Mahdi Zavvari, male, Iran, PhD. Research fields focus on nanostructure based photodetectors, single photon avalanche photodiodes, and graphene based photodetectors. E-mail: m. zavvari@ iaurmia. ac. ir

impress the performance of QRIP. On the other hand, since the QRs are doped layers, the thermally generated dark current in absorption region might be in higher orders which can degrade the detectivity.

One way to increase the performance of a QRIP, is to enhance the amplitude of optical incidence within active region. This can be achieved either by reflecting the photons back into the active region via additional layers or by increasing the absorption peak for selected wavelengths by excitation of plasmonic waves[18]. In this paper, resonant cavity enhanced-resonant tunneling-quantum ring inter-subband photodetector (RCE-RT-QRIP) is proposed to improve the performance of the detector. In such structure, Al_2O_3/GaAs distributed bragg reflectors (DBR) are used to confine the optical field within active region of detector and to enhance the quantum efficiency and thereby increase the responsivity. For further improvement, the dark current of detector should be reduced. In our proposed structure $Al_{0.3}Ga_{0.7}As$/ $In_{0.3}Ga_{0.7}As$ resonant tunneling barriers are included in absorbing layers to reduce dark current of device. For such detector it is expected to have higher specific detectivity compared to conventional QRIPs. In this paper we analyze and simulate the performance characteristics of proposed detector to show its improved operation.

The paper is organized as follows: In section 2, theoretical model of QRIP, resonant cavity structure and resonant tunneling barriers are presented and the results of simulations are given in section 3. Finally, the paper is concluded in section 4.

1 Theoretical model

1.1 Inter-subband absorption coefficient

To characterize QRIP performance, first the wavefunctions and energy levels within QRs must be obtained. In order to obtain electronic energy states and wavefunctions within QR conduction band, we use effective mass approximation to solve 3D Schrödinger equation for quantum rings. The Hamiltonian is written as:

$$H_e = P\frac{1}{2m_e^*(x,y,z)}P + V_e(x,y,z) \quad , \quad (1)$$

in which:

$$V(x,y,z) = \begin{cases} 0, (R_i)^2 \leqslant x^2 + y^2 \leqslant (R_o)^2, |z| \leqslant h \\ E_c, \text{other} \end{cases} \quad (2)$$

and

$$m^*(x,y,z) = \begin{cases} m_i, (R_i)^2 \leqslant x^2 + y^2 \leqslant (R_o)^2, |z| \leqslant h \\ m_o, \text{other} \end{cases} \quad (3)$$

where E_c is the conduction band offset between ring and barrier materials and m_i and m_o are electron mass in ring and barrier. R_i, R_o and l are quantum ring inner and outer radius and height, respectively. According to prior studies, the bandgap energy of an InAs ring under higher strain changes from 0.77 eV to 0.513 eV[19]. The other important effect of strain is that the effective mass is energy and position dependent because of non-parabolic energy bands. The modified effective mass can be calculated from the relation[20]:

$$\frac{1}{m_e(r,E)} = \frac{p^2}{\hbar^2}\left(\frac{2}{E + E_g(r) - V_e(r)} - \frac{1}{E + E_g(r) - V_e(r) + \Delta(r)}\right) \quad , \quad (4)$$

where p is momentum, E is electron energy, E_g is bandgap energy, and Δ is split-off energy. Equations 1 and 4 are solved for InAs/GaAs material system by an iterative procedure considering the effects of strain to obtain the electronic energy states and wavefunctions within the ring. Inter-subband absorption coefficient for a single layer InAs/ GaAs QRs is equal to [21]:

$$a(\hbar\omega) = \frac{\pi q^2}{\varepsilon_0 n_0 c m_0^2 V_{ac}} \cdot \frac{1}{\hbar\omega}\sum |\bar{a}, P_{fi}|^2 N(\hbar\omega) \quad (5)$$

where V_{ac} is effective volume of a QR layer, $\bar{a}$ is incidence light polarization vector, P_{fi} momentum matrix element and N is density of states which can be calculated from [22]:

$$N(\hbar\omega)\int_{-\infty}^{\infty}\frac{\hbar\gamma_{fi}/\pi}{(E-E')^2 + (\hbar\gamma_{fi})} \times \frac{1}{\sqrt{2\pi}\sigma} \exp\left(\frac{-(E_{fi}-E')^2}{(\sqrt{2}\sigma\gamma_{fi})^2}\right) \times (f_i(E') - f_f(E'))\,dE' \quad ,(6)$$

where E_{fi} is transition energy of subbands. In calculation of density of states, effect of some broadening mechanisms is included. Because of non-uniformity in size and shape of rings, a Gaussian function is considered to introduce inhomogeneous broadening with energy of σ. In addition, thermal effects and scattering mechanisms lead to homogeneous broadening of energy states which is modeled by a Lorentzian function with line-width of $\hbar\gamma_{fi}$. For simplicity we assumed that the Fermi level lies between ground and first excited state to ensure that there is at least one electron in initial state which can optically excite and occupy the upper final state.

1.2 DBR reflectivity and transmission

In order to increase the optical field inside the active region of detector, one way is to use DBR as the bottom reflector of resonant cavity structure. DBR consists of stacked layers of different materials with variable refractive index. These layers act as a dielectric mirror that

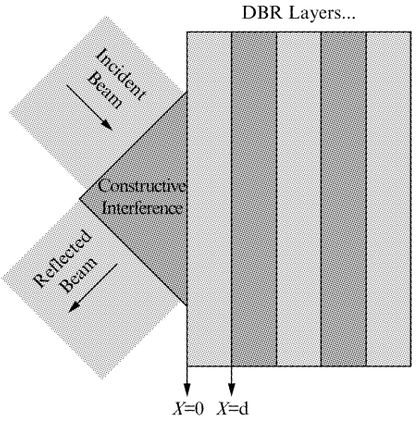

Fig. 1 Constructive interference of reflected beams from DBR layers

reflects back the radiations of selected wavelength. Such selectivity is a result of difference between refractive indices (Δn) of layers. The reflected and transmitted beam are considered as electric and magnetic fields which are satisfied the boundary conditions of DBR layers shown in figure 1 and are calculated using transfer matrix method (TMM). The amplitude of electric and magnetic field at the boundary of $x=0$ and $x=d$ can be related to each other by 2×2 transfer matrix as follow[23]:

$$\begin{bmatrix} E_a \\ B_b \end{bmatrix} = M_1 \begin{bmatrix} E_b \\ B_b \end{bmatrix} \quad , \quad (7)$$

and for N layer of DBR structure we have:

$$\begin{bmatrix} E_a \\ B_b \end{bmatrix} = M_T \begin{bmatrix} E_N \\ B_N \end{bmatrix} \quad , \quad (8)$$

$$M_T = M_1 M_2 M_3 \cdots M_N \rightarrow M_1 = \begin{pmatrix} \cos\delta & \frac{i\sin\delta}{\gamma_1} \\ i\gamma_1 \sin\delta & \cos\delta \end{pmatrix} \quad . (9)$$

So, the reflection (r) and transmission (t) coefficient are defined as:

$$t = \frac{2\gamma_0}{\gamma_0 m_{11} + \gamma_0\gamma_s m_{12} + m_{21} + \gamma_s m_{22}},$$
$$r = \frac{\gamma_0 m_{11} + \gamma_0\gamma_s m_{12} - m_{21} - \gamma_s m_{22}}{\gamma_0 m_{11} + \gamma_0\gamma_s m_{12} + m_{21} + \gamma_s m_{22}} . \quad (10)$$

Using resonant cavity structure, the quantum efficiency (QE) for a photodetector can be increased as [24]:

$$\eta = \left\{ \frac{(1+R_2 e^{-ad})}{1 - 2\sqrt{R_1 R_2} e^{-ad} \cos(2\beta L + \varphi_1 + \varphi_2) + R_1 R_2 e^{-2ad}} \right\} \times (1 - R_1)(1 - e^{-ad}) \quad , \quad (11)$$

where d is the effective absorption region width modified by coverage factor (ξ) of QRs, R_1 and R_2 are reflectivity of the bottom and top reflector, φ_1 and φ_2 are phase shift, L is the cavity length and β is the corresponding propagation constant. The responsivity of a detector is defined as the ratio of output photocurrent (Ip) to optical input power (P_{in}) and can be obtained from[25]:

$$R = \frac{I_p}{P_{in}} = \frac{e}{\hbar\omega}\eta g \quad , \quad (12)$$

where g is the photoconductive gain which is equal to $g = \frac{1 - p_c/2}{FNp_c}$ where N is the number of QR layers, P_c is capture probability and F is a fill factor. For proposed structure, two periods of Al_2O_3/GaAs layers are used as bottom DBR mirror with $\Delta n \sim 2$. A thin layer of Au is also deposited on top of structure to capture the radiations reflected from DBRs within active region. This leads to increased absorption probability in active region and hence the responsivity is elevated.

1.3 Dark current and detectivity

Dark current of a quantum ring photodetector is originated from thermal excitation of electrons which are drifted under applied electric field and reached the contacts at no incident and can be calculated from [26]:

$$I_D(V) = q \cdot n(V) \cdot v(V) \cdot A \quad , \quad (13)$$

where $v(V)$ is the average electron drift velocity in the barrier material, A is the detector area and $n(V)$ is density of thermally generated electrons which can be calculated from[26]:

$$n(V) = \int N(E) \cdot f(E) \cdot T(E,V) \cdot dE \quad , (14)$$

where $f(E)$ is Fermi-Dirac distribution function, $T(E, V)$ is the transmission probability through device and $N(E)$ is the density of states expressed by[26]:

$$N(E) = \sum_i \frac{2N_D}{Lp} \frac{1}{\sqrt{2\pi\sigma}} \exp\left(\frac{(E - E_i)^2}{2\sigma^2} \right) + \frac{4\pi m^*}{Lp\hbar^2} H(E - E_w) + \frac{8\pi\sqrt{2}}{\hbar^3} m^{*3/2} \sqrt{E - E_c} H(E - E_c) \quad , (15)$$

where N_D is the density of quantum dot surface, L_p is the absorption length, E_i is the energy levels within QR and $H(E)$ is the step function. The first term in equation (15) corresponds to density state of QR, the second term expresses the wetting layer density of states which E_w is wetting layer energy level and the last term describes barrier bulk density of states with conduction bandage energy of E_c.

Specific detectivity (D^*) of a photodetector is a main parameter used to rate its performance and its higher orders is required. Detectivity is proportional to responsivity and inverse of dark current of photodetector. So, in our proposed detector by lowering the dark current and increasing the responsivity higher detectivity can be obtained. Specific detectivity is related to responsivity and dark current of photodetector using the relation of[27]:

$$D^* = R\frac{\sqrt{A\Delta f}}{i_n} \quad , \quad (16)$$

where Δf is the bandwidth, R is responsivity and in is the noise current of the device and is equal to $i_n = \sqrt{4qI_D g_n \Delta f}$ where g_n is noise gain.

The schematic of proposed RCE-RT-QRIP and one period of its conduction band diagram are shown in figure 2. InAs QRs with dimensions of 2 nm, 8 nm and 35 nm as height, inner radius and outer radius, respectively are embedded in GaAs matrix inside the active region of photodetector. According to figure 2, a resonant tunneling filter is also included in active region to stop the thermally electrons from contribution in current generation and hence lower the dark current. Huang et al. has reported

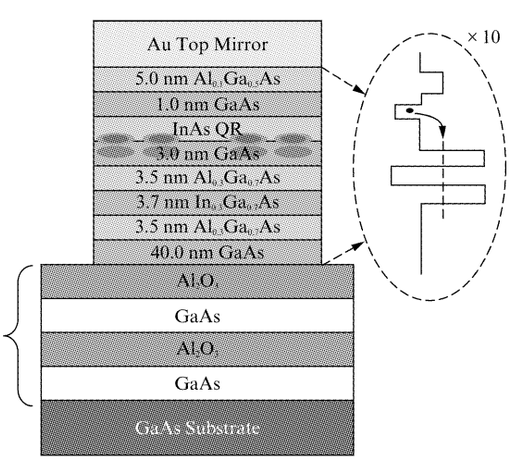

Fig. 2　Schematic of RCE-RT-QRIP layers. (Inset shows the conduction band diagram of one stack of active region)

using resonant tunneling barrier to reduce dark current of QRIP [28]. Actually inclusion of RT barrier leads to creation of a photocurrent pass and therefore only the photogenerated carriers are allowed to pass and contribute in current generation. Hence one can expect lower dark currents while the photocurrent and responsivity remain unchanged. In this paper, the effect of resonant tunneling barriers on dark current and detectivity of InAs/GaAs QRIP is investigated.

2 Results and discussion

Solution of Schrodinger equation gives an inter-subband transition energy about 0.015 5 eV corresponding to wavelength of 80 μm (3.75 THz). Using the equation 5, we calculate inter-subband absorption for QR layers and results are shown in Figure 3. As we expect, absorption peak occurs at the wavelength of 80 μm and based on this operation wavelength, DBR layers are designed to reflect the transmitted radiations back. The reflection of DBR layers is calculated considering the number of BDR layers, refractive indices of layers and operation wavelength. In order to increase the probability of absorption in active region, high reflectivity of DBR layer is desired. Assuming quarter-wavelength rule, the thickness of layers should be in the order of several μm. Since the multiple layers in DBR results in increased thickness of whole structure which might accompany with some difficulties in fabrication process, large difference between refractive indices of DBR materials is required. For this purpose, we choose Al_2O_3/GaAs as DBR layers due to higher refractive indices difference ($\Delta n \sim 2$). Recently, Wang and Lin have reported performance characteristics of quantum dot infrared photodetector with Al_2O_3/GaAs DBR considering fabrication procedure[29]. Using 2 pairs of Al_2O_3/GaAs, the reflection of DBR layers is obtained about approximately 90% and therefore one can expect an increase on absorption and QE spectrum. Figure 3 also shows the reflection of DBR layers and it can be seen that reflection peak of DBR layers occur in identical wavelength. We assume refractive index of 3.34 for GaAs and 1.34 for Al_2O_3 which gives a thickness of ~5.9 μm and ~14.9 μm for DBR materials based on quarter-wavelength rule. To further confinement of optical field, a thin layer of Au material is used as top reflector with reflection coefficient of about 90% for wavelength of 80 μm.

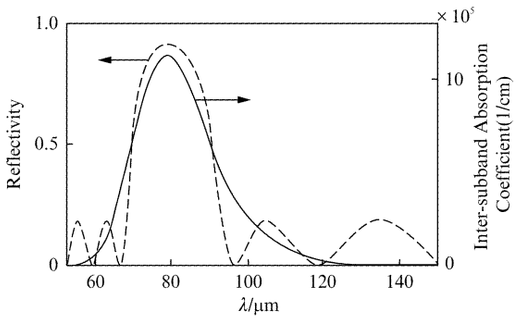

Fig. 3 Inter-subband absorption of QR layers and reflection of QRIP vs. wavelength

Figure 4 shows the reflection of DBR layer as a function of DBR period at 80 μm wavelength. According to figure 4, the reflection of DBR can be reached to ~99% using 3 periods of Al_2O_3/GaAs layers, however this results in increased thickness of structure which causes more complexity in growth and fabrication process. Also from practical point of view, it may be difficult to grow up thick DBR due to higher levels of strain. Hence we set two periods of DBR layers for our structure. The calculated responsivity and QE spectrum for device are shown as a function of wavelength in figure 5. According to figure, QE of 1.3% can be achieved using RCE structure. This value for QE can enhance the responsivity of device considerably. As can be seen, for 10 stack of QR within active region, responsivity of photodetector is about 0.4(A/W) which is one order of magnitude higher than experimental results reported in [17].

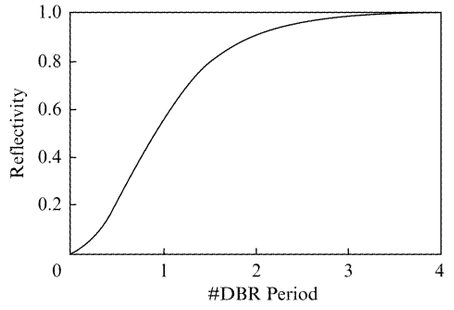

Fig. 4 Reflectivity of DBR layers versus the number of Al_2O_3/GaAs layers

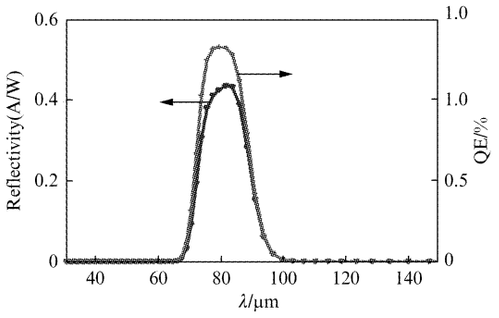

Fig. 5 Responsivity and quantum efficiency of device as a function of wavelength

On the other hand to reduce the dark current, two $Al_{0.3}Ga_{0.7}As$ barriers with an $In_{0.3}Ga_{0.7}As$ middle well are used as resonant tunneling barrier in active region of QRIP. Calculated dark current density considering RT barriers is shown in figure 6 as a function of bias voltage and for different temperatures. According to figure, dark current is in higher levels for increased applied bias as a result of higher drift velocity. On the other hand, for higher temperatures, dark current rapidly increases which describe thermally nature of generated dark carriers. Such an increase in dark current results in reduction of overall performance and hence the operation temperature of QRIP. Results show that the dark current density at 0.4 V is in the order of 10^{-9}, 10^{-7} and 10^{-5} A/cm^2 for 80, 100 and 120 K, respectively.

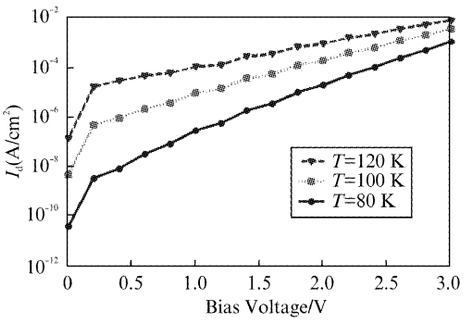

Fig. 6 Calculated dark current density of RT based device for different temperatures vs. bias

Figure 7 illustrates the calculated specific detectivity for RCE-RT InAs/GaAs QRIP and conventional QRIP as a function of applied bias for two different temperatures. Because of domination of dark current, for higher bias voltage the specific detectivity takes lower values. It's the case for higher temperatures which cause a reduction in detectivity curve. According to figure, D^* of RCE-RT-QRIP is in the order of $\sim 10^{11}$ and $\sim 10^{10}$ (cm. Hz$^{1/2}$/W) for temperature of 80 and 120 K, respectively. It is evident that D^* of RCE-RT-QRIP is two orders of magnitude higher than conventional QRIP at same temperatures.

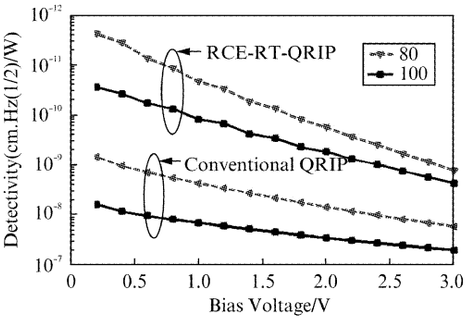

Fig. 7 Calculated D^* of RCE-RT-QRIP and conventional QRIP for different temperature as a function of bias voltage

To better evaluation of proposed RCE-RT-QRIP, the performance characteristic of conventional QRIP, RCE-QRIP and RT-QRIP are investigated and compared with RCE-RT-QRIP in table 1 at the same operation wavelength. Results show that, combination of resonant cavity structure with resonant tunneling barrier can improve all characteristic of conventional QRIP including QE, responsivity, dark current and detectivity, while other structure can't cover all of parameters. As can be seen from table, RT-QRIP improves the dark current and specific detectivity of conventional QRIP considerably, but responsivity of conventional QRIP remains unchanged. On the other hand, RCE-QRIP can enhance the responsivity of conventional QRIP as much as four times, while it can't affect dark current of device. However, detectivity of RCE-RT-QRIP is two orders of magnitudes higher than the specific detectivity of conventional QRIP.

Table 1 Comparison the characteristic performance of conventional QRIP, RT-QRIP, RCE-QRIP and RCE-RT-CRIP at 80 μm

Parameter	QE	Responsivity (A/W)	I_d(T=80 K)	D^*(T=80 K)
Conventional QRIP	0.3%	0.1	$\sim 10^{-7}$(A/cm^2)	$\sim 10^{8}$(cm. Hz$^{1/2}$/W)
RT-QRIP	0.3%	0.1	$\sim 10^{-9}$(A/cm^2)	$\sim 10^{10}$(cm. Hz$^{1/2}$/W)
RCE-QRIP	1.3%	0.4	$\sim 10^{-7}$(A/cm^2)	$\sim 10^{10}$(cm. Hz$^{1/2}$/W)
RCE-RT-QRIP	1.3%	0.4	$\sim 10^{-9}$(A/cm^2)	$\sim 10^{11}$(cm. Hz$^{1/2}$/W)

3 Conclusion

Performance characteristics of a resonant tunneling InAs/GaAs quantum ring inter-subband photodetector embedded in resonant cavity structure were studied and results were compared with conventional QRIP. Proposed QRIP shows the inter-subband absorption coefficient peak at 80 μm wavelength. According to the results, resonant cavity structure considerably enhanced the responsivity and quantum efficiency of device. Specific detectivity of device was calculated in the order of $\sim 10^{11}$ (cm. Hz$^{1/2}$/W) at the wavelength of 80 μm and T = 80 K which is considerably higher than the specific detectivity of a conventional QRIP.

References

[1] Rostami A, Rasooli H, Baghban H. *Terahertz Technology* [M]. Springer, 2011.

[2] Siegel P H. Terahertz technology in biology and medicine [J]. *Microwave Theory and Techniques, IEEE Transactions on*, 2004, **52**(10): 2438-47.

[3] Liu H, Song C, Springthorpe A, *et al*. Terahertz quantum-well photodetector [J]. *Applied physics letters*, 2004, **84**(20): 4068-70.

[4] Skalare A, Mcgrath W R, Echternach P M, *et al*. Aluminum hot-electron bolometer mixers at submillimeter wavelengths [J]. *Applied Superconductivity, IEEE Transactions on*, 2001, **11**(1): 641-4.

[5] Cai X, Jenkins G, Sushkov A, *et al*. Graphene terahertz photodetector [J]. *Bulletin of the American Physical Society*, 2012, **57**(1).

[6] Su X, Yang J, Bhattacharya P, *et al*. Terahertz detection with tunneling quantum dot intersublevel photodetector [J]. *Applied physics letters*, 2006, **89**(3): 031117-3.

[7] Hsu B-C, Lin C-H, Kuo P-S, *et al*. Novel MIS Ge-Si quantum-dot infrared photodetectors [J]. *Electron Device Letters, IEEE*, 2004, **25**(8): 544-6.

[8] Krishna S, Kwon O-H, Hayat M M. Theoretical investigation of quantum-dot avalanche photodiodes for mid-infrared applications [J]. *Quantum Electronics, IEEE Journal of*, 2005, **41**(12): 1468-73.

[9] Zavvari M, Ahmadi V. Dynamics of avalanche quantum dot infrared photodetectors [J]. *Modern Physics Letters B*, 2012, **26**(32): 1250216-10.

[10] Zavvari M, Ahmadi V. Quantum-dot-based mid-IR single-photon detector with self-quenching and self-recovering operation [J]. *Electron Device Letters, IEEE*, 2013, **34**(6): 783-5.

[11] Lin W H, Tseng C C, Chao K P, *et al*. InGaAs-capped InAs-GaAs quantum-dot infrared photodetectors operating in the long-wavelength infrared range [J]. *Photonics Technology Letters, IEEE*, 2009, **21**(18): 1332-4.

[12] Zavvari M, Ahmadi V, Mir A, *et al*. Quantum dot infrared photodetector enhanced by avalanche multiplication [J]. *Electronics letters*, 2012, **48**(10): 589-91.

[13] Carr G L, Martin M C, Mckinney W R, *et al*. High-power terahertz

radiation from relativistic electrons [J]. Nature, 2002, **420**(6912): 153-6.
[14] Mittleman D M, Jacobsen R H, Nuss M C. T-ray imaging [J]. *Selected Topics in Quantum Electronics, IEEE Journal of*, 1996, **2**(3): 679-92.
[15] Sherwin M. Applied physics: Terahertz power [J]. *Nature*, 2002, **420**(6912): 131-3.
[16] Bhowmick S, Huang G, Guo W, *et al*. High-performance quantum ring detector for the 1-3 terahertz range [J]. *Applied Physics Letters*, 2010, **96**(23): 231103-3.
[17] Lee J H, Dai J H, Chan C F, *et al*. In (Ga) As quantum ring terahertz photodetector with cutoff wavelength at 175 [J]. *Photonics Technology Letters, IEEE*, 2009, **21**(11): 721-3.
[18] Wang L, Chen X, Hu W, *et al*. The resonant tunability, enhancement, and damping of plasma waves in the two-dimensional electron gas plasmonic crystals at terahertz frequencies [J]. *Applied Physics Letters*, 2013, **102**(24): 243507-5.
[19] Li S S, Xia J B. Electronic states of InAs/GaAs quantum ring [J]. *Journal of Applied Physics*, 2001, **89**(6): 3434-7.
[20] Wang W, Hwang T M, Jang J C. A second-order finite volume scheme for three dimensional truncated pyramidal quantum dot [J]. *Computer physics communications*, 2006, **174**(5): 371-85.
[21] Kochman B, Stiff-Roberts A D, CHAKRABARTI S, *et al*. Absorption, carrier lifetime, and gain in InAs-GaAs quantum-dot infrared photodetectors [J]. *Quantum Electronics, IEEE Journal of*, 2003, **39**(3): 459-67.
[22] Mir A, Ahmadi V. Design and analysis of a new structure of InAs/GaAs QDIP for 8-12 μm infrared windows with low dark current [J]. *Journal of Modern Optics*, 2009, **56**(15): 1704-12.
[23] YEH P. *Optical waves in layered media* [M]. Wiley New York, 1988.
[24] UNLU M S, STRITE S. Resonant cavity enhanced photonic devices [J]. Journal of Applied Physics, 1995, **78**(2): 607-39.
[25] LIU H. Quantum dot infrared photodetector [J]. Optoelectronics Review, 2003, **11**(1): 1-5.
[26] SU X, CHAKRABARTI S, BHATTACHARYA P, *et al*. A resonant tunneling quantum-dot infrared photodetector[J]. Quantum Electronics, IEEE Journal of, 2005, **41**(7): 974-9.
[27] TOWE E, PAN D. Semiconductor quantum-dot nanostructures: Their application in a new class of infrared photodetectors [J]. Selected Topics in Quantum Electronics, IEEE Journal of, 2000, **6**(3): 408-21.
[28] HUANG G, GUO W, BHATTACHARYA P, *et al*. A quantum ring terahertz detector with resonant tunnel barriers [J]. Applied Physics Letters, 2009, **94**(10): 101115-3.
[29] WANG C-C, LIN S-D. Resonant cavity-enhanced quantum-dot infrared photodetectors with sub-wavelength grating mirror [J]. Journal of Applied Physics, 2013, **113**: 213108-6.